Journal of Applied Polymer Science

Structure and morphology of nanoporous ZnO and dark current-voltage characteristics of the glass/(TCO)/ZnO/poly[2,7-(9,9-dioctylfluorene)-*alt*-(5,5′-bithiophene)/Ag structure

Lidia Ghimpu,[1] Tamara Potlog,[2] Ana-Maria Resmerita,[3] Ion Tiginyanu,[1] Aurica Farcas[3]

[1]Institute of Electronic Engineering and Nanotechnologies, Academy of Sciences of Moldova, MD-2028 Chisinau, Republic of Moldova

[2]Moldova State University, Chisinau, MD-2009, Republic of Moldova

[3]"Petru Poni" Institute of Macromolecular Chemistry, Gr. Ghica Voda Alley 41A, 700487 Iasi, Romania

Correspondence to: A. Farcas (E-mail: auricafarcas@yahoo.com)

ABSTRACT: The hybrid organic-inorganic structure based on glass/(TCO)/nanoporous ZnO/poly[2,7-(9,9-dioctylfluorene)-*alt*-(5,5′-bithiophene)]/Ag that was prepared by physical deposition has been investigated. The structure of the nanostructured ZnO obtained by magnetron sputtering was confirmed by X-ray diffractometry (XRD) and energy dispersive X-ray spectroscopy (EDX). Scanning electron microscopy (SEM) analysis proved the existence of short and interconnected zinc oxide (ZnO) fibers, which form a continuous porous network with pores having an average diameter of 100 nm. Current-voltage (I-V) curves of the glass/TCO/ZnO/PF-BT/Ag hybrid structure are similar to those of typical *p-n* junctions and stable until 90°C temperature. According to the I-V characteristics, the dominant mechanism of current flow is based on the generation-recombination of carriers in the depletion region at low direct biases and also on the injection of carriers at high biases. The reverse branch of the I-V characteristic, calculated in log-log scale, shows one segment with a power coefficient of 3/2 at room temperature. © 2015 Wiley Periodicals, Inc. J. Appl. Polym. Sci. **2015**, *132*, 42415.

KEYWORDS: conducting polymers; microscopy; morphology; nanostructured polymers; porous materials

Received 17 December 2014; accepted 22 April 2015

DOI: 10.1002/app.42415

INTRODUCTION

Transparent conductive oxides (TCO) thin films, such as indium tin oxide (ITO),[1] zinc oxide (ZnO),[2] and antimony tin oxide (ATO),[3] have been widely used as transparent cathodes in opto-electronic devices due to their low resistivity, high visible transmittance, and high infrared reflectance. Despite the dominant practical applications of ITO in optoelectronic devices, ZnO has also received considerable attention owing to its relevant properties such as similar electron affinity, band gap (E_g=3.37 eV) and large exciton binding energy (60 meV),[4] a hexagonal structure which allows optical refraction,[5] high electron mobility, as well as chemical and thermal stability.[6] Over the last years, ZnO nanostructures attracted increasing interest as photoanode in dye-sensitized solar cells (DSSCs) prompting the requirement for multiple transport and injection layers.[7–9] In many cases, the efficiency of solar to electrical power conversion was improved by controlling the morphology and particle size of ZnO nanostructures.[10,11]

Conjugated polymers (CP) have also gained wide attention as alternative materials for transparent conductive layers, because of their application in a great variety of hybrid ZnO nanorod solar cells. Until now, several CP/ZnO solar cells have been reported but the devices exhibited low conversion efficiency.[12–17] Among the various CP, poly[2,7-(9,9-dioctylfluorene)-*alt*-(5,5′-bithiophene)] alternating copolymers (PF-BT) have suitable properties, such as slight tendency of intermolecular interactions, higher tendency to organize into fibers, reversible doping capability through an electrochemical process, as well as good solubility in organic solvents and the transparency of solid films.[18] In addition, they exhibit good hole transporting properties based on thermotropic liquid crystallinity, which allows better chain packing via self-assembly.[19] Therefore, PF-BT copolymers appear to be one of the most promising organic semiconducting materials capable to generate an innovative hybrid device.[20,21]

Herein, we report the investigation of the temperature effect on the dark I-V characteristics of a glass/TCO/ZnO/PF-BT/Ag configuration. The proposed hybrid structure is based on nanofibrous ZnO as *n*-type semiconductor,[22] coated with PF-BT as hole transfer layer. To the best of our knowledge, the

dependency of the dark I-V with temperature of the glass/TCO/ZnO/PF-BT/Ag hybrid structure has not been studied yet.

EXPERIMENTAL

Materials

9,9-Dioctylfluorene-2,7-bis(trimethyleneborate) (97%), 5,5′-dibromo-2,2′-bithiophene, bromobenzene (99%), and tetrakis (triphenylphosphine) palladium (99%) were purchased from Sigma-Aldrich and used as received. Commercial analytical grade solvents were used without further purification.

Synthesis of PF-BT Copolymer

PF-BT alternating copolymer was prepared by Suzuki cross-coupling polymerization of 9,9-dioctylfluorene-2,7-bis(trimethyleneborate) (**1**) and 5,5′-dibromo-2,2′-bithiophene (**2**) in toluene.[23] At the end of reaction a slight excess of monomer **1** was added, followed by bromobenzene (Br-Ph) as monofunctional end-capping reagent instead of 3-bromothiophene.[24] Subsequently, the reaction mixture was cooled to room temperature, the solution was filtered and the filtrate was poured into a mixture of methanol/deionized water (10/1 v/v). The fibrous material was recovered by filtration through a funnel, and washed sequentially with water, methanol, and acetone. After being dried under reduced pressure at 60°C, the solid was purified by Soxhlet extraction with acetone for 48 h with a view to remove oligomers and the catalyst. The copolymer was obtained as an orange solid in 49% yield.

^{1}H-NMR (400 MHz, $CDCl_3$, δ): 7.70–7.60 (m, 6H, fluorene), 7.51–7.34 (m, 4H, bithiophene), 7.24 (m, Ph), 2.07 (s, 4H, dioctyl), 1.11–1.10 (m, 24H, dioctyl), 0.81–0.79 (d, 6H, dioctyl).

^{13}C-NMR (100 MHz, $CDCl_3$, δ): 151.83–139.88, 132.82, 121.52–119.80 (aromatic carbons from fluorene), 136.53, 132.82–128.78, 127.19–123.69 (aromatic carbons from bithiophene), 55.36, 40.41, 31.80, 29.99, 29.71, 23.80, 14.06 (aliphatic carbons from fluorene).

IR (KBr): $\nu = 3422$, 2926, 2854, 1733, 1450, 1261, 1096, 1022, 880, 836, 798, 741, 700, 633, 542.

GPC (THF, Pst standard): $M_n = 14{,}700$, $M_w/M_n = 1.46$.

Synthesis of a Nanofibrous ZnO

The detailed synthesis of a nanofibrous ZnO material by the magnetron sputtering technique has been described elsewhere.[9] Pure porous ZnO was deposited over SnO_2 thin films with a surface of 1.5 cm^2 on glass substrates by radio-frequency (rf) magnetron sputtering. The main advantage of method consists in the high speed of layer deposition, as well as good reproducibility and accuracy of the composition of the deposited layers. Basic parameters of the rf magnetron sputtering method are the magnetron frequency and power, the gas pressure in the working chamber and the magnetic induction. The synthesis rate in magnetron sputtering depends on the power of the discharge current and the gas pressure in the working chamber. We succeeded to grow ZnO layers using a disc of 99.99% pure zinc as target, in argon (Ar) atmosphere by applying rf and power, according to an earlier reported procedure.[9] First, the substrates were cleaned for 2–3 h in a solution containing 7 g $K_2Cr_2O_7$, 10 ml H_2O, and 100 ml H_2SO4 at room temperature. The Ar pressure was kept constant at 7.4 10^{-3} mbar. The magnetron power was 200 W, and the deposition time was 120 min. The substrate was kept at 110°C throughout the procedure. Several sets of samples were prepared following this protocol. These ZnO nanolayers grown on tin oxide/glass substrate were afterwards introduced in a reactor and annealed at 490°C for 45 min, under an oxygen (O_2) atmosphere with a flow of approximately 100 cm^3 min–1.

Preparation of a Glass/TCO/ZnO/PF-BT/Ag Hybrid Structure

Next, PF-BT layers were deposited onto the TCO/ZnO substrates by spin-coating from a concentrated tetrahydrofuran (THF) solution. In the hybrid structure, Ag was used as a top electrode and TCO as a bottom electrode. In this configuration, electrons are collected at the bottom electrode, while the top electrode collects the holes.[25]

Measurements

The chemical structure of PF-BT copolymer was proved by ^{1}H NMR (Bruker Avance DRX 400 MHz) and IR (Specord Carl Zeiss Jena). The molecular weight was determined by gel permeation chromatography (GPC) using a PL-EMD 950 Evaporative Mass Detector instrument and THF as elution solvent. Thermal stability was investigated by thermogravimetric analysis (TGA) and differential scanning calorimetry (DSC) on a Mettler Toledo TGA/SDTA 851e balance and Mettler Toledo DSC-1, respectively. Cyclic voltammetry (CV) was carried out in a three-electrode cell using platinum (Pt) working electrode, a Pt-wire counter-electrode, and silver (Ag) wire pseudo-reference electrode.[18] The supporting electrolyte was a 0.01M solution of tetrabutylammonium hexafluorophosphate ($TBAPF_6$) in acetonitrile (ACN). The thin layer of PF-BT copolymer obtained by casting on the working electrode from THF solution was then scanned in the interval −2.3 and +1.2 V vs. Ag.[18] Photoluminescence (PL) measurements were performed with a time-correlated single photon counting (TCSPC) spectrometer using a pulsed diode laser (Edinburg Instruments-EPL-375) at 371 nm as excitation source and a cooled photomultiplier (Becker & Hickl PMC-100-1) coupled to a monochromator and TCSPC electronics (Edinburg Instrument Lifespec-ps TCC-900 PC card). The PL efficiency was measured using a relative method for optical dilute solutions, employing the quantum yield of quinine sulfate decahydrate in 0.5M sulfuric acid as reference (Φ= 54.6±5%). Atomic force microscopy (AFM) experiments were performed using a Digital Instruments Dimension 3100 AFM (Veeco Company) equipped with a Nanoscope IV controller. Standard silicon cantilevers with a spring constant between 4.4–44 Nm^{-1} were used in the tapping mode. Advancing and receding contact angle measurements on spin-coated PF-BT films were performed by using the drop shape analysis profile device equipped with a tiltable plane (DSA-P, Kruss, Germany). Ultrapure water (Millipore, resistivity=18 MΩ cm) or a diiodomethane drop was first deposited on the sample using a variable volume micropipette. The drop volume was set to 15 μL for water and 10 μL for diiodomethane. In order to perform dynamic contact angle measurements, the sample surface sustaining the drop was tilted at a constant speed (1 deg s^{-1}) and the images of the drop were simultaneously

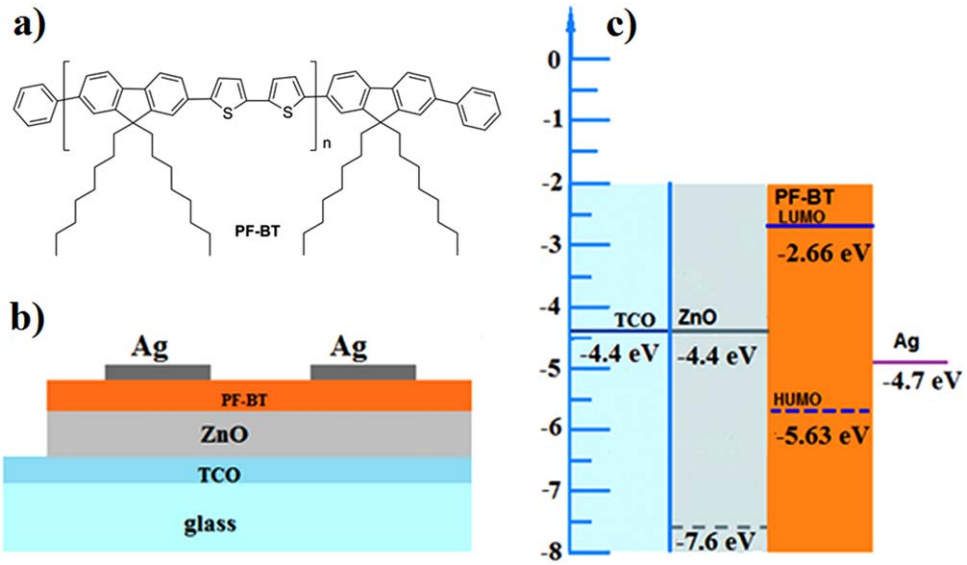

Figure 1. (a) The chemical structure of PF-BT copolymer; (b) the schematic representation of the hybrid structure; and (c) energy levels of the investigated hybrid structure. [Color figure can be viewed in the online issue, which is available at wileyonlinelibrary.com.]

recorded.[18] The advancing contact angle was measured at the front edge of the drop, just before the triple line starts moving. The phase structure of the deposited nanoporous ZnO films was studied using a Rigaku X-ray diffractometer (XRD) (CuK_α radiation (λ=1.54178 Å)) under optimized operating conditions of 30 mA and 40 kV at a scanning rate of 0.04° s^{-1} in the 2θ range of 24–90°. The morphology and the chemical composition of the nanostructured ZnO films were studied using a TESCAN Scanning Electron Microscope (SEM) equipped with an Oxford instruments INCA energy dispersive X-ray (EDX) system for chemical composition analysis. The EDX analysis of the obtained structures afforded the relative stoichiometric ZnO composition (within a precision of 1%). I-V characteristic curves of the device were measured at different temperatures using a Keithley 2400 power supply under dark conditions.

RESULTS AND DISCUSSION

Physico-Chemical Characteristics of PF-BT Alternating Copolymer

The high tendency of PF-BT to organize into fibers,[18] as well as its good ability to form highly transparent solid films recommend it for the investigation as hole transfer layers in organic-inorganic hybrid structures. The chemical structure of PF-BT and schematic representation of the glass/TCO/ZnO/PF-BT/Ag structure is shown in Figure 1.

PF-BT macromolecular compound was prepared by Suzuki cross-coupling reaction from **1** and **2** in a 1/1 molar ratio.[23] A small excess of **1** was then added, and finally, Br-Ph was used as a monofunctional end-capping reagent to introduce phenyl groups at both polymer chain ends.[26] The chemical structure of the investigated copolymer was confirmed by IR and NMR spectroscopy. It should be mentioned that PF-BT shows good solubility in common organic solvents such as $CHCl_3$, CH_2Cl_2, THF, and toluene. The copolymer's determined number-average molecular weight (M_n), as estimated by GPC analysis, was approximately 15,000 g mol^{-1} with a polydispersity index (PDI) of 1.4. It is worth mentioning that M_n and PDI have to be considered merely indicative, due to the rigid rod-like structure of the copolymer. The thermal properties of PF-BT copolymer were evaluated by TGA and DSC analysis. TGA data revealed that the compound was stable up to 300°C.[18] The DSC curve on the second heating scan of the PF-BT sample exhibited a glass transition temperature (T_g) at 75°C.

The Photophysical Properties of PF-BT Copolymer

The UV-vis spectrum of PF-BT copolymer showed a maximum beyond 510 nm, which corresponded to the π–π^* transition of the copolymer backbone.[18] In addition, the time-resolved PL exhibited well-defined vibronic structures with a predominance of the 0–0 transitions and an energy difference of 0.16 eV. The optical properties of PF-BT macromolecular compound revealed no significant aggregation. The fluorescence lifetimes followed a mono-exponential decay with a value $\tau = 630 \pm 30$ ps. The HUMO/LUMO energy levels clearly indicated that PF-BT copolymer is electrochemically accessible in an electroluminescence configuration cell. The surface topography of spin-coated film from a dilute THF solution onto silicon-oxide substrates was investigated by AFM and confirmed a rod-like structure of the compound.[18] It is important to note that the rod-like structures form loops as a result of the macromolecular chains flexibility. The values of the surface free-energy with its dispersive (γ_s^d) and polar (γ_s^p) components obtained for the spin-coated copolymer film indicated a typical surface covered with a close packing of hydrocarbon chains.[27] The photovoltaic characteristics in a bulk heterojunction solar cell of a blend between PF-BT copolymer and [6,6]-phenyl-C_{61}-butyric acid methyl ester (PCBM) in a 1/1 w/w ratio indicated lower efficiency, either as a consequence of the low absorption of light or due to moderate molecular weights of copolymer, which could diminish the device performance.[28]

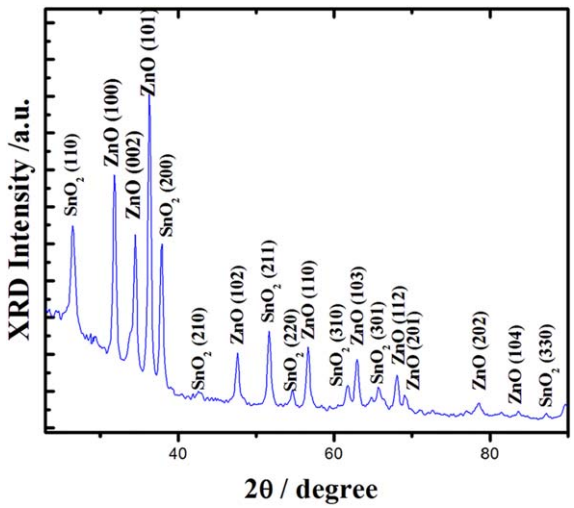

Figure 2. XRD patterns of nanoporous ZnO grown by magnetron sputtering at 5°C on TCO/glass substrate (The TCO substrate peaks are marked and are assigned to SnO_2, according to PDF 00–041-1445 card). [Color figure can be viewed in the online issue, which is available at wileyonlinelibrary.com.]

Structural Characterization of the Nanostrucured ZnO

The crystalline structure of the nanostrucured ZnO was investigated by XRD. The XRD pattern of doped nanoporous ZnO films is shown in Figure 2.

The diffraction peaks in the pattern can be indexed to hexagonal wurtzite structured ZnO (space group: $P6_3mc(186)$; a=0.3249 nm, c=0.5206 nm), and diffraction results are in good agreement with the JCPDS 036–1451 card for ZnO.[29] The intensity of the peaks relative to the background signal demonstrates the high purity of the ZnO hexagonal phase and a very good crystallinity of the samples grown by magnetron sputtering.[30–32] The absence of characteristic peaks for impurities is an indication of a single hexagonal ZnO phase, as shown in Figure 2.

Table I. The Chemical Composition of ZnO Nanofiber

Element	Weight %	Atomic %
O K	24.25	57.27
Zn K	71.70	41.44
Sn L	4.05	1.29
Total	100.0	

Morphological Properties of the Nanostrucured ZnO Thin Films

Data concerning the chemical composition of the nanostructured ZnO thin films were derived from the EDX spectrum [Figure 3(a)], and the results are summarized in Table I. The ZnO samples contained 41.44% Zn and 57.27% O_2.

The porous and homogenous of ZnO layer surface is clearly reflected in the SEM images [Figure 3(b,c)]. It can be clearly seen that ZnO nanofibers are relatively uniform, which indicates a small size variation. The short fibers are interconnected and form a continuous porous network with pores having an average diameter of 100 nm [Figure 3(b)]. The nodes of intersection

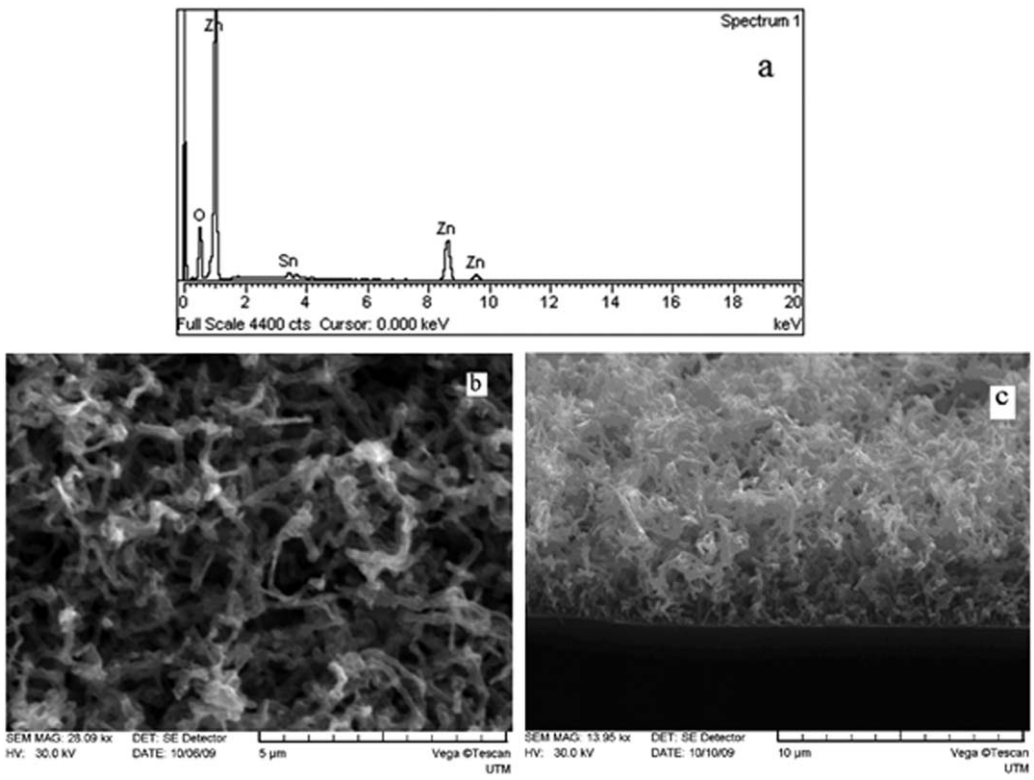

Figure 3. (a) EDX images of nanoporous ZnO; (b,c) SEM images of nanoporous ZnO films grown by magnetron sputtering on TCO/glass substrate; top and cross-sectional views, respectively. Scale bars are 5 µm and 10 μm, respectively.

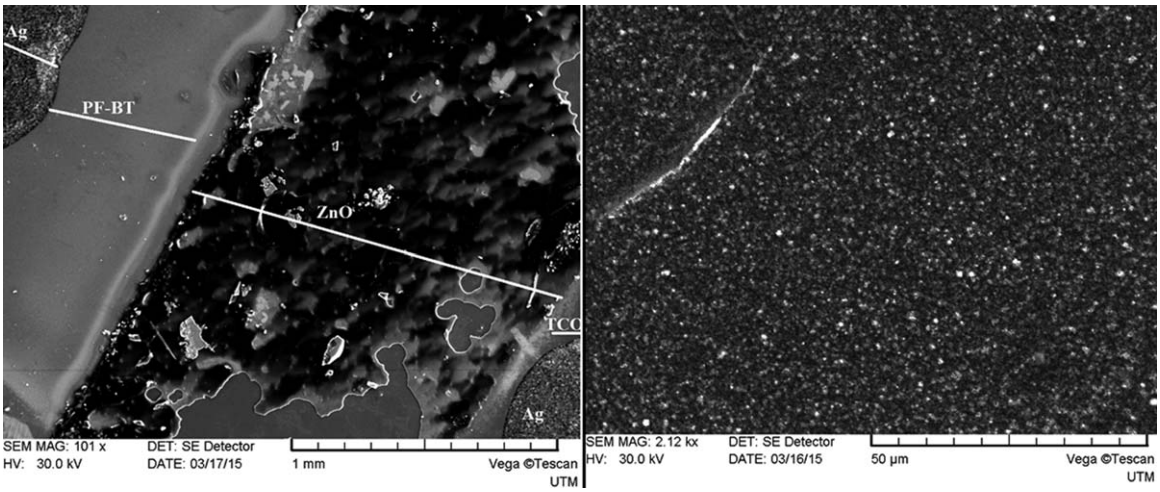

Figure 4. SEM image of TCO/ZnO/PF-BT with (left) and without top electrode (right).

of nanowires exhibited sizes ranging from 250 to 800 nm. A similar trend was also observed in the SEM images of TCO/ZnO/PF-BT with and without a connection with the top electrode, (Figure 4). The TCO/ZnO/PF-BT in connection with the top electrode had a less homogeneous surface [Figure 4(left)], while the surface without connection was more homogeneous and almost devoid of irregularities [Figure 4(right)]. The data strongly suggests that the PF-BT copolymer was deposited outside of ZnO and did not penetrate deep into the ZnO nanofibers, thus proving unhindered accessibility only on the surface of nanoporous ZnO. The nodule size in TCO/ZnO/PF-BT samples does not change significantly.

Effect of Temperature on the I-V Characteristics Curves of the Glass/TCO/ZnO/PF-BT/Ag Structure

The I-V characteristics curves are the most important parameter of power semiconductors, and the curves are temperature-dependent.[33] The dark I-V characteristics of the glass/TCO/ZnO/PF-BT/Ag structure were measured in a temperature range from 20 to 110°C, with a temperature step of 10°C, by applying voltage to the bottom electrode. Because of overlaps, a better destruction of law can be observed only after the curves corresponding to 50, 60, 70, and 80°C have been omitted (Figure 5). A gradual increase of the direct current was obtained in the investigated range of temperature. Furthermore, the structure displays significantly rectification behavior in the dark, and the forward direction of current increases exponentially with the bias of voltage (Figure 5). It should be mentioned that a *p-n* junction with a depletion region at the interface was detected for most studied interfaces of inorganic/organic layers.[34,35]

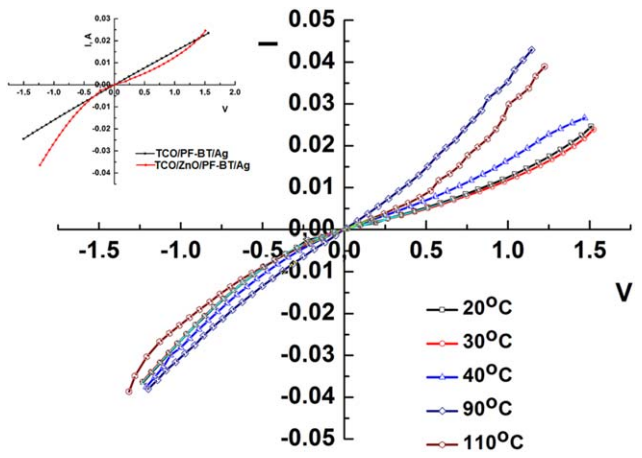

Figure 5. Dark I-V characteristics of the glass/TCO/ZnO/PF-BT/Ag structure measured in the temperature range between 20 and 110°C with a step of 10°C. The temperature dependence of TCO/PF-Bt/Ag without ZnO is reported in the inset. [Color figure can be viewed in the online issue, which is available at wileyonlinelibrary.com.]

Qualitatively, it can be envisaged that such behavior is similar to those of a real diode.[36,37] As it can be seen from the temperature dependence of TCO/PF-Bt/Ag without ZnO, the behavior similar to that of a real diode disappears, [Figure 5(inset)]. This observation prompted us to describe the I-V characteristics of the investigated hybrid structure using eq. (1):

$$I = I_s\left(\exp\frac{eV}{nkT} - 1\right) \quad (1)$$

where I_s is the device saturation current, n the ideality factor, k is Boltzmann's constant, and T is temperature.

We have found that an increase in temperature from 20 to 90°C augments both the forward and the reverse I. In addition, the rectification coefficient also increases from 0.5 to ~2 within the same temperature range, while at temperatures higher than 90°C, in both directions I decreases. This phenomenon could be presumably assigned to changes in the morphological properties of PF-BT copolymer upon exposure to temperatures above its glass transition.[38] Also, it was found that barrier height values decrease from 0.25 to 0.16 eV within the same temperature range.

Further insight is provided by extracting the diode parameters from semi-logarithmic I-V plots (Figure 6), as well as from n and I_s values, as determined from eq. (1). It is noteworthy that the value of n increases from 1 to 2 at low voltage (i.e. <0. 4 V).

Furthermore, the I_s value was estimated by extrapolating the forward current curves $lnI = f\ (V)$ to V=0. Additional

information concerning the variations of I_s with temperature was obtained from eq. (2). I_s values were found to vary exponentially with $\frac{1}{T}$ in the measured temperature range.

$$I_s(T) \approx I_{oo}\exp\left(-\frac{\Delta E_A}{kT}\right) \quad (2)$$

where ΔE_A is the activation energy of the charge carriers in the forward bias.

A value of 0.828 eV for ΔE_A was calculated as the slope of lnI_s versus $1/T$ from the direct I-V dependencies. An analysis of n and ΔE_A values suggested that the generation-recombination of carriers in the depletion region can be responsible for the dark current. At high voltage (i.e. >0.4 V), the value of n varies between 11 and 18, and all the characteristics show a sublinear behavior. The results presented here may be explained on the basis of the theory of injection depletion.[34,35] The dependence is probably related to the effect which takes place when diffusion of the injected carriers is directed contrary to the drift current. Such results obtained in a wide range of temperature suggest a drift-diffusion model of the current transport. We also noticed that when the structure is reversing biased, the I-V characteristics curves can be described by low power, according to eq. (3).

$$I \approx V^m \quad (3)$$

where m is power coefficient.

The reverse branch of the I-V characteristic (calculated in log-log scale) shows one segment, whose power coefficient m is 3/2 at room temperature (Figure 7).

As shown in Figure 7, the value of m decreases to 1 when temperature increases to 110°C. It should be pointed out that the value is comparable with the activation energy determined from the direct I-V dependencies. We also noted that the temperature dependence of the reverse current of I-V segment exhibited an activation nature. These results can be associated with the participation of the same deep centers in the charge transfer in direct and reverses biases.

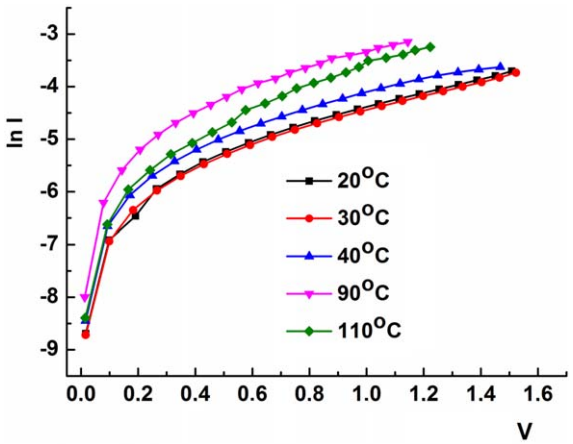

Figure 6. Direct I-V dependencies of the glass/TCO/ZnO/PF-BT/Ag structure measured in the temperature range between 20 and 110°C. [Color figure can be viewed in the online issue, which is available at wileyonlinelibrary.com.]

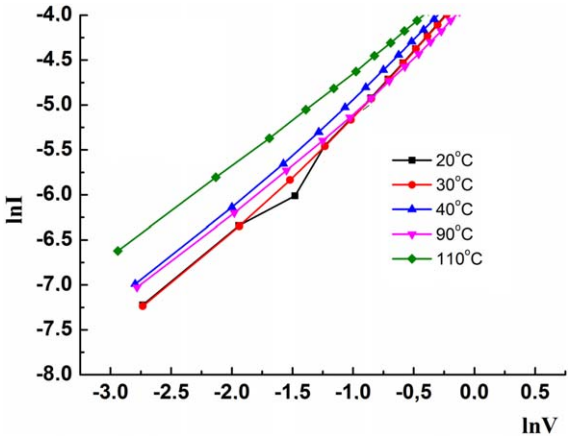

Figure 7. Reverse I-V dependencies of the glass/TCO/ZnO/PF-BT/Ag structure measured in the temperature range from 20 to 110°C. [Color figure can be viewed in the online issue, which is available at wileyonlinelibrary.com.]

CONCLUSIONS

Structural and morphological properties of TCO/nanoporous ZnO thin films, as well as dark I-V characteristics curves of the hybrid organic-inorganic configuration were investigated. XRD pattern of ZnO layers successfully grown on TCO/glass substrate using magnetron sputtering method indicated a single hexagonal ZnO phase. SEM and EDX images of ZnO layers exhibited a porous and mainly homogenous structure over the whole surface. The dark I-V characteristics of the glass/TCO/ZnO/PF-BT/Ag hybrid structure at different temperatures are similar to those of real diodes. For low voltage values, the rectification coefficient increases from 0.5 to ~2 in the temperature range 20–90°C. These experimental results suggest that at high voltage values, the diode parameters can be obtained by taking into account the theory of injection depletion. The temperature dependence of the reverse current exhibited an activation nature, and its value is comparable with the activation energy determined from direct I-V dependence. This would suggest the participation of the same deep centers in the charge transfer in direct and reverse biases.

ACKNOWLEDGMENTS

This work was financially supported by grants from the Romanian National Authority for Scientific Research, CNCS – UEFISCDI, projects PN-II-ID-PCE-2011-3-0035, PN-II-CT-RO-MD-2012-1 (2012–2014), and from the Supreme Council for Science and Technological Development of the Academy of Sciences of Moldova.

REFERENCES

1. Helander, M. G.; Wang, Z. B.; Qiu, J.; Greiner, M. T.; Puzzo, D. P; Liu, Z. W.; Lu, Z. H. *Science* **2011**, *332*, 944.
2. Shin, Y.-H.; Cho, C.-K.; Kim, H.-K. *Thin Solid Films* **2013**, *548*, 641.
3. Luo, L.; Bozyigit, D.; Wood, V.; Niederberger, M. *Chem. Mat.* **2013**, *25*, 4901.

4. Ku, C. H.; Wu, J. J. *Appl. Phys. Lett.* **2007**, *91*, 93117.
5. Lee, K. H.; Cho, N. I.; Yun, E. J.; Nam, H. G. *Appl. Surf. Sci.* **2010**, *256*, 4241.
6. Lao, C. S.; Park, M. C.; Kuang, Q.; Deng, Y.; Sood, A. K.; Polla, D. L.; Wang, Z. L. *J. Am. Chem. Soc.* **2007**, *129*, 12096.
7. Yun, S.; Lim, S. *J. Solid State Chem.* **2011**, *184*, 273.
8. Li, S.; Zhang, X.; Jiao, X.; Lin, H. *Mater. Lett.* **2011**, *65*, 2975.
9. Lupan, O.; Guérin, V. M.; Ghimpu, L.; Tiginyanu, I. M.; Pauporté, T. *Chem. Phys. Lett.* **2012**, *550*, 125.
10. Ito, S.; Kitamura, T.; Wada, Y.; Yanagida, S. *Sol. Energy Mat. Sol. Cells* **2003**, *76*, 3.
11. Kim, S. S.; Yum, J. H.; Sung, Y.-E. *J. Photochem. Photobiol. Chem.* **2005**, *171*, 269.
12. Beek, W. J. E.; Sloff, L. H.; Wienk, M. M.; Kroon, J. M.; Janssen, R. A. J. *Adv. Funct. Mater.* **2005**, *15*, 1703.
13. Beek, W. J.; Wienk, M. M.; Janssen, R. A. J. *Adv. Mater.* **2004**, *16*, 1009.
14. Krebs, F. C.; Thomann, Y.; Thomann, R.; Andreasen, J. W. *Nanotechnology* **2008**, *19*, 424013.
15. Ravirajan, P.; Peiró, A. M.; Nazeeruddin, M. K.; Graetzel, M.; Bradley, D. D. C.; Durrant, J. R.; Nelson, J. *J. Phys. Chem. B* **2006**, *110*, 7635.
16. Wang, L.; Zhao, D.; Su, Z.; Shen, D. *Nanoscale Res. Lett.* **2012**, *7*, 106.
17. Lira-Cantu, M.; Krebs, F. C. *Sol. Energy Mater. Sol. Cells* **2006**, *90*, 2076.
18. Farcas, A.; Tregnago, G.; Resmerita, A.-M.; Dehkordi-Taleb, S.; Cantin, S.; Goubard, F.; Aubert, P.-H.; Cacialli, F. *J. Polym. Sci. Part A: Polym. Chem.* **2014**, *52*, 460.
19. Gather, M. C.; Bradley, D. D. C. *Adv. Funct. Mater.* **2007**, *17*, 479.
20. Ravirajan, P.; Haque, S. A.; Durrant, J. R.; Poplavskyy, D.; Bradley, D. D. C.; Nelson, J. *J. Appl. Phys.* **2004**, *95*, 1473.
21. Jo, J.; Vak, D.; Noh, Y.-Y.; Kim, S.-S.; Lim, B.; Kim, D. Y. *J. Mater. Chem.* **2008**, *18*, 654.
22. Pandey, A. K.; Nunzi, J.-M.; Wang, H.; Oey, C. C.; Djurisic, A. B.; Xie, M. H.; Leung, Y. H.; Man, K. K. Y.; Chan, W. K. *Org. Electron.* **2007**, *8*, 396.
23. Stefanache, A.; Silion, M.; Stoica, I.; Fifere, A.; Harabagiu, V.; Farcas, A. *Eur. Polym. J.* **2014**, *50*, 223.
24. Farcas, A.; Resmerita, A.-M.; Stefanache, A.; Balan, M.; Harabagiu, V. *Beilstein J. Org. Chem.* **2012**, *8*, 1505.
25. Lattante, S. *Electronics* **2014**, *3*, 132.
26. Farcas, A.; Jarroux, N.; Harabagiu, V.; Guegan, P. *Eur. Polym. J.* **2009**, *45*, 795.
27. Cantin, S.; Bouteau, M.; Benhabib, F.; Perrot, F. *Colloids Surf. A* **2007**, *276*, 107.
28. Bijleveld, J. C.; Zoombelt, A. P.; Mathijssen, S. G. J.; Wienk, M. M.; Turbiez, M.; de Leeuw, D. M.; Janssen, R. A. J. *J. Am. Chem. Soc.* **2009**, *131*, 16616.
29. American Society for Testing and Material, Powder Diffraction Files, Joint Committee on Powder Diffraction Standards, Swarthmore: PA, **1996**; p 3.
30. Lupan, O.; Chow, L.; Chai, G.; Roldan, B.; Naitabdi, A.; Schulte, A.; Heinrich, H. *Mater. Sci. Eng. B* **2007**, *145*, 57.
31. Chow, L.; Lupan, O.; Chai, G. *Phys. Status Solidi B* **2010**, *247*, 1628.
32. Lupan, O.; Chow, L.; Chai, G.; Heinrich, H. *Chem. Phys. Lett.* **2008**, *465*, 249.
33. Antohe, S. In Phase Transitions. Applications to Liquid Crystals, Organic Electronic and Optolelectronic Fields; Popa-Nita, V., Ed.; Research Signpost, 2006; Chapter 10, p 189.
34. Antohe, S. In Phase Transitions. Applications to Liquid Crystals, Organic Electronic and Optolelectronic Fields; Popa-Nita, V., Ed.; Research Signpost, 2006; Chapter 11, p 210.
35. Beek, W.; Wienk, M.; Janssen, R *Adv. Mater.* **2004**, *16*, 1009.
36. Sze, S. M.; Kwok, K. N. In Physics of Semiconductor Devices, 3rd ed.; Sze, S. M.; Kwok, K. N., Eds.; Wiley: New Jersey, **2007**; Chapter 2, p 79.
37. Baranovskii, S. D.; Faber, T.; Hensel, F.; Thomas, P. *J. Phys. Condens. Matter* **1997**, *9*, 2699.
38. Liao, Y.-M.; Shih, H.-M.; Hsu, K.-H.; Hsu, C.-S.; Chao, Y.-C.; Lin, S.-C.; Chen, C.-Y.; Meng, H.-F. *Polymer* **2011**, *52*, 3717.